Vertical Flight Society's Design-Build-Vertical Flight Competition Final Technical Report Submission

Caleb Brady[1], Joseph Ferrari[1], Simon Fox[1], Nathaniel Hahn[2,3], Danyal Sainz-Gootenberg[1], Joshua Paine[1], Majid Rashidi[1], Isabella Zimmer[4], Amos Langsner[1], Andrew Ali[2], Ashraf Ibraheem[2], Brandon Kuo[1], Brian Keys[1], Brian Nyirenda[2], Donovan Crowley[2], Erik Anell[1], Gavin Rauh[1,5], Jacob Slater[1], Lincoln Reiter[1], Matthew Trout[1], Michael Bastuga[1], Mitchell Schultz[1], Willis Erdman[2]

1 Dept. of Aerospace and Mechanical Engineering, Case Western Reserve University, Cleveland, OH 44106
2 Dept. of Electrical, Computer, and Systems Engineering, Case Western Reserve University, Cleveland, OH 44106
3 Dept. of Computer and Data Science, Case Western Reserve University, Cleveland, OH 44106
4 Dept. of Biomedical Engineering, Case Western Reserve University, Cleveland, OH 44106
5 Dept. of Economics, Case Western Reserve University, Cleveland, OH 44106

Date: 3 March 2025

1 Executive Summary

1.1 Objective Statement

Our objective is to engineer, manufacture, and fly a drone that can compete in the VFS DBVF (Vertical Flight Society Design-Build-Vertical Flight competition), emphasizing stability and controllability to benefit all four missions' parameters, with a primary focus on maximizing payload capacity, endurance, and repeatability.

1.2 Purpose of Design

The design challenge centers on creating an unmanned aircraft that serve as subscale demonstrators for AAM (advanced air mobility) in the VFS DBVF competition. The key design requirements focus on showcasing the aircraft's capabilities in terms of range, agility, speed, payload capacity, and payload dropping accuracy, to ultimately serve as a functional firefighting tool. We have designed our aircraft with the ability to carry 14-18 8-ounce water bottles as to satisfy flight mission 2 (FM2). The overall objective is a stable drone with long loiter times and high capacity in order to facilitate success in competition missions, and in applicability to real-world firefighting use.

1.3 Planned Approach

Our design is a standard hexacopter utilizing the Pixhawk 6X pro-Flight Controller and an RTK module, with a primary focus on optimizing payload capacity and endurance for superior performance in the competition's FM1 and FM2. Payload capacity is managed through a weight distribution strategy and the design of the propulsion subsystem. The propulsion subsystem is specifically engineered to facilitate the flight of a 25-pound drone, the competition's maximum gross weight limit. For the payloads, 8-ounce water bottles will be centered around the CG of the aircraft. Additionally, the actuation and order of payload dropping have been thoroughly deliberated in order to minimize CG variation during drops. Our mission model MATLAB script closely monitored the aircraft's parameters. Optimization algorithms were used to find ideal motor-prop-battery combinations. The electronics design is focused on reliability and positional accuracy. We employed Electronic Speed Controller (ESC) telemetry to aid with PID tuning, additionally using load cells and tethered testing to corroborate motor data. Furthermore, we emphasized the modularity of components for ease of repair and design iteration.

2 Management Summary

2.1 Gantt Chart

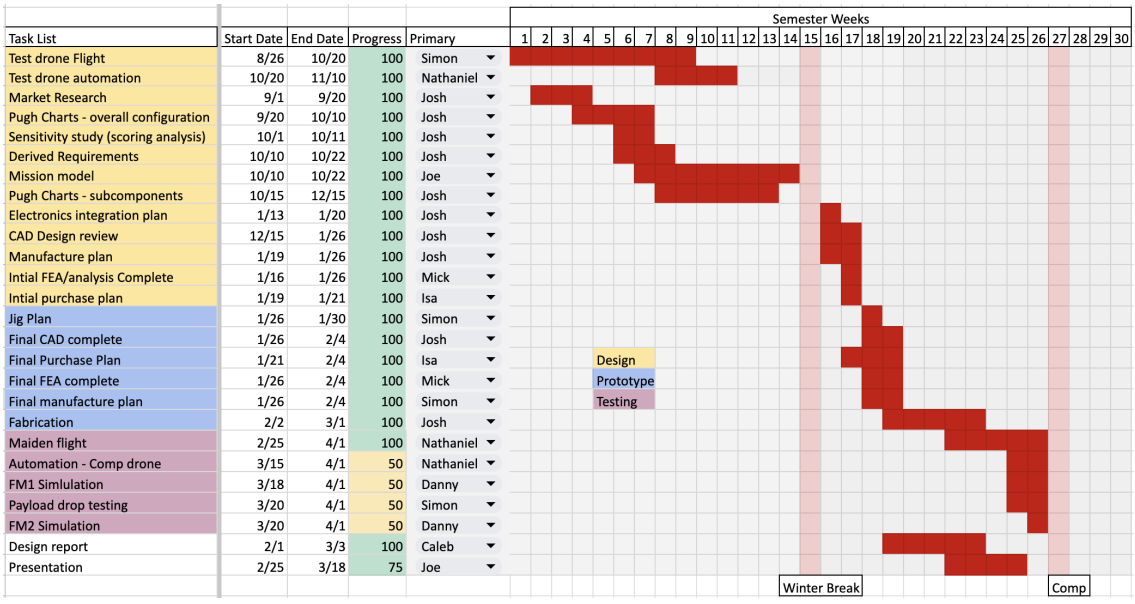

Task List	Start Date	End Date	Progress	Primary
Test drone Flight	8/26	10/20	100	Simon
Test drone automation	10/20	11/10	100	Nathaniel
Market Research	9/1	9/20	100	Josh
Pugh Charts - overall configuration	9/20	10/10	100	Josh
Sensitivity study (scoring analysis)	10/1	10/11	100	Josh
Derived Requirements	10/10	10/22	100	Josh
Mission model	10/10	10/22	100	Joe
Pugh Charts - subcomponents	10/15	12/15	100	Josh
Electronics integration plan	1/13	1/20	100	Josh
CAD Design review	12/15	1/26	100	Josh
Manufacture plan	1/19	1/26	100	Josh
Intial FEA/analysis Complete	1/16	1/26	100	Mick
Intial purchase plan	1/19	1/21	100	Isa
Jig Plan	1/26	1/30	100	Simon
Final CAD complete	1/26	2/4	100	Josh
Final Purchase Plan	1/21	2/4	100	Isa
Final FEA complete	1/26	2/4	100	Mick
Final manufacture plan	1/26	2/4	100	Simon
Fabrication	2/2	3/1	100	Josh
Maiden flight	2/25	4/1	100	Nathaniel
Automation - Comp drone	3/15	4/1	50	Nathaniel
FM1 Simlulation	3/18	4/1	50	Danny
Payload drop testing	3/20	4/1	50	Simon
FM2 Simulation	3/20	4/1	50	Danny
Design report	2/1	3/3	100	Caleb
Presentation	2/25	3/18	75	Joe

2.2 Team Structure

Member	Role	Email	Class
Caleb Brady	Chief Engineer	Caleb.Brady@case.edu	Senior
Joseph Ferrari	President	Joseph.Ferrari@case.edu	Senior
Lincoln Reiter	Risk Manager	Lincoln.Reiter@case.edu	Senior
Mitchell Schultz	PR Chair	Mitchell.Schultz@case.edu	Senior
Isabella Zimmer	Treasurer	Isabella.zimmer@case.edu	Senior
Nathaniel Hahn	Electronics Lead	Nathaniel.Hahn@case.edu	Junior
Joshua Paine	Mechanical Lead	Joshua.Paine@case.edu	Senior
Simon Fox	Testing Lead	Simon.Fox@case.edu	Sophomore
Danyal Sainz-Gootenberg	Pilot 1	Dns47@case.edu	Senior
Gavin Rauh	Pilot 2	Gavin.Rauh@case.edu	Freshman
Dr. Majid Rashidi	Advisor	Mxr268@case.edu	-

3 Business Case Study

3.1 Background Research

Wildfires, especially in recent years, have come to the forefront of world news, with the impact of wildfires experienced in unpopulated land reservations and populated areas alike steadily growing more severe. Many of these wildfires would be preventable with early detection and mitigation before they progress but can't easily be put out with conventional firefighting means. Currently, satellites are a main contributor to early wildfire detection. The federal government has approved expanded funding to utilize the National Oceanic and Atmospheric Association (NOAA) for this purpose. "NOAA satellites play a pivotal role in fire detection, mapping, and environmental impact assessment.: These capabilities support firefighting agencies in making informed decisions, allocating resources efficiently, and forecasting fire behavior with predictive models." [1]

With these current practices in mind, drones have already begun to, play a pivotal role in early detection. Corroborating NASA and NOAA, a study, "Airborne Optical and Thermal Remote Sensing for Wildfire Detection and Monitoring," in the National Library of Medicine, says, "satellite visit periods are often too infrequent and image resolution inadequate for detection of fires when they are small and developing." [2] Instead, they highlight unmanned aerial vehicles as a promising "intermediary solution" between fixed detection facilities and satellites.

3.2 Flight Mission Scenario

Although early detection has been used with effectiveness, we believe early action is a logical next step for unmanned aerial vehicles in fire protection. Flight mission two, with the precision dropping of liquid payloads, would facilitate not only detection with a sensor and navigation suite but also the ability to extinguish budding fires before they would be typically detectable with current practices.

3.3 Target Market

Although diverse markets around the world would benefit from an unmanned vehicle capable of dropping small payloads in otherwise inaccessible areas, the National Park Service (NPS), the US Forest Service (USFS), and the Bureau of Land Management (BLM), with their recent injection of 1 billion federal dollars for wildfire prevention from the infrastructure investment and jobs act [3], are our initial customers of focus. With the flexibility and ease of use of semi-autonomous drones, forest rangers on the ground could implement our drone technology as the end-users, preventing the need to hire dedicated pilots in an already resource-deprived organization.

3.4 Value Proposition

As publicly funded organizations, where operations cannot be driven by profit, value is paramount. The early detection enabled by drones will ensure that resources are allocated where they should be. Hot-spot detection will streamline the response of traditional firefighting solutions. However, beyond the value-add from strategic resource allocation, our drone is capable of delivering a precision payload, with a potential value upside of 560 Million Dollars

3.4.1 First-Response

With the advanced infrared and optic sensor package, which interfaces with our aircraft, a payload of fire retardant, delivered strategically in a capsule, could put out a large portion of wildfires before they are even recognizable by traditional means. According to the Smithsonian, up to 45% of human-caused wildfires start from a localized incident, such as a wayward campfire ember. Additionally, up to 84% of wildfires domestically are human-caused [4], meaning precise GPS navigation enabling travel to a human-flagged location could quickly extinguish fires. If even half of these fires were extinguished, it could result in a 19% yearly decrease.

3.4.2 In-Situ Antivenom Delivery Package

In addition to fire detection and first response, it would be remiss to neglect other value streams enabled by our aircraft. Each year, dozens succumb, and 8000 more are injured due to untreated venomous animal bites while exploring national parks. [5] With precision payload dropping capability and a universal dropper attachment, antivenom packages could be delivered to a large portion of those victims, preventing liability, reducing trepidation for potential customers, and, most importantly, saving lives. It's important to note that emergency rescue costs up to 10000 dollars per hour, so any reduction becomes highly valuable.

	Before implementing our aircraft	After	Reduction
Wildfire cost to USFS per year (M$)	2900	2349	551
Invasive Species cost per year (M$)	19	9.5	9.5
Totals (M$)	2,919	2,358.5	560.5

Figure 1: Numerical value summary [6][7]

3.4.3 Invasive Species Detection Capability

The advanced optics package required for fire detection and early warning easily interfaces with AI recognition software. Flora enthusiasts use applications such as Google Lens to identify plant species from just a photo. The same package coud interface with our optics system to identify hotbeds of invasive species growth prone to fire in the future. Beyond early detection and fast reaction, predictive modeling could reduce wildfires before they even start by focusing forest management efforts. Predictive maintenance, being the most cost-effective form, would provide major value to forest service in reducing future costs and resource strain.

4 Design Trade Studies

4.1 Sensitivity study

When designing a VTOL for wildfire suppression, optimizing performance aspects is crucial. A sensitivity study evaluated payload capacity, speed, and endurance, identifying payload and endurance as the primary drivers. While higher speed improves response time, the mission's short travel distances (max 400 ft) reduce its impact. Instead, endurance is critical to maximize operational efficiency within the 10-minute flight limit. A drone that cannot remain airborne for the full duration wastes potential payload delivery time. Flight Mission 2 prioritizes delivering firefighting payloads, making payload capacity essential. A higher payload reduces resupply trips, maximizing point-scoring opportunities. However, increasing payload inherently trades off with speed and endurance. Balancing these trade-offs, the team prioritizes payload while ensuring 10-minute endurance. Speed remains a consideration, but sustained payload delivery is the key to effective wildfire suppression.

4.2 Mission requirements

The requirements we outlined are meant to include real tangible goals, often including number targets, which you can see in column 1 of figure 2. To frame our analysis of the RFP, we broke our requirements into multiple categories/subsystems: Aircraft design, Mission parameters, Electronics Design, Safety, and Budget. The third column of our table serves as an in-depth descriptor of the requirement, providing context and rationale to the specific number stated in column 1. Additionally, we broke our requirements into customer, customer/derived, and derived requirements. This breakdown shows our shift from first quantifying the RFP to deriving our own goals for our drone. The derived requirements either stem from customer requirements defined by the RFP or are based on conventional drone guidelines found through market research and team experience.

Requirement	Category/subsystem	Description/Justification	Requirement Type
Reload time must be under 4 minutes total	Mission Parameter	Conform to competition guidelines	Customer
Drone Complies with General FAA laws and practices	Safety	Keep spectators, team members and all participants of the VFS DBF safe at all times	
Must conform to VTOL DBF flight safety standards	Safety	Keep spectators, team members and all participants of the VFS DBF safe at all times (Ex. valid shunt plug location, Geofence)	
All Electronics will be compliant with FAA and VFS rules	Electronics Design	For maximum safety and success at competititon, all protocols will be followed (Ex. valid shunt plug for propulsion and radio systems, FAA module, 6s lipo battery)	
overall weight should be around 25 lbs	Mission Parameter	Maximize points during FM2, conform to competition guidelines	
Fly for 10 minutes with Max payloads	Aircraft Design/Mission Parameter	Maximize points during FM2, conform to competition guidelines	Customer/ derived
Fly for 15 minutes without payloads	Aircraft Design/Mission Parameter	Maximize points during FM1, conform to competition guidelines	
3:1 Thrust to weight ratio	Aircraft Design/Mission Parameter	Guarantee that the drone has ample mobility/maneuverability to complete both FM1 and FM2. Keeping in mind the downside to more thrust: higher cost, higher loads, often less efficient.	Derived
Must be able to carry upwards of 12 payloads	Aircraft Design	Maximize points during FM2, striking a balance between efficiency, loading time and consistency throughout the mission	
Must have at least one spare for every part on the drone, which is identical	Aircraft Design	For maximum redundancy multiple copies of all parts will be fabricated, while keeping in mind modularity and the resources at hand	
Total Cost Under 10,150$	Budget	Given funding from multiple student associations in the past, this is a projected total engineering budget for the year	
Under 1mm of total deflection	Aircraft Design	Given vibration and PID problems associated with tuning large drones, this will be a critical requirement for responsiveness	
Land Safely at 40 cm/sec	Aircraft Design	Ardupilot automated mission recommends landing at around this speed: good baseline for safe and controlled landing	
Main plate must be less than 12"x12"	Aircraft Design	Taking into account common accessible stock material, common manufacturing sizing limits and cost contrainst this serves as a good outline for sizing	
Must be minimum 8 g/W efficiency at hover [fully loaded]	Aircraft Design	Considering FM2 and the possible long flight times with increased weight, effiency is paramount and our drone should be optimized largely around this feature	

Figure 2: Derived requirements

4.3 Review of Overall Configurations

Drone Configuration				X-4		X-8		Hexacopter		TriCopter		Octocopter		Tri-6	
Evaluation Criteria	Specifics	Target	Weight	Raw Score	Weighted Score	Raw Score	Weighted Score	Raw Score	Weighted Score	Raw Score	Weighted Score	Raw Score	Weighted Score	Raw Score	Weighted Score
Performance	Speed	Maximize top speed	0.05	3	0.15	4	0.2	2.5	0.125	2.5	0.125	1	0.05	4	0.2
	Acceleration	Maximize acceleration	0.05	3	0.15	4	0.2	3	0.15	2	0.1	3.5	0.175	3	0.15
Payload	Lifting Capacity	Maximize relative payload weight	0.2	2	0.4	3	0.6	3	0.6	0	0	4	0.8	2	0.4
	Airframe	Allow for good payload attatchment	0.05	4	0.2	4	0.2	4	0.2	4	0.2	4	0.2	4	0.2
Stability	Control	Maximize controlability	0.2	3.5	0.7	3	0.6	4	0.8	1	0.2	4	0.8	1	0.2
Range	Battery performance	Maximize range	0.2	4	0.8	3	0.6	4	0.8	4	0.8	4	0.8	4	0.8
Cost	Manufacturing	Maximize ease of manufacture	0.1	4	0.4	3	0.3	3.5	0.35	3	0.3	3.5	0.35	3	0.3
	Material Cost	Minimize component cost	0.1	4	0.4	1	0.1	2	0.2	4	0.4	0	0	3	0.3
Redundancy	System Failure Response	Maximize redundancy	0.05	0	0	4	0.2	3	0.15	0	0	3	0.15	3	0.15
Weighted Total Score			1		3.2		3		3.375		2.125		3.325		2.7

Figure 3: Overall configuration PUGH decision matrix

During the consideration of various subsystems, Pugh charts supported by research were utilized to select the optimal choices based on overall desired performance metrics. The rating system for the Pugh charts spans from 0 to 4, with 0 being unsatisfactory, 1 being just tolerable, 2 being acceptable, 3 being satisfactory, and 4 being exceptional. The team decided to consider six different design configurations for our overall configuration: X-4, X-8, Hexacopter, Tricopter, Octocopter, and Tri-6.

Before creating the Pugh matrix, the mission parameters were analyzed, and the team quickly ruled out any configuration that involved traditional flight surfaces, change in flight phase, or rotating motors. The necessity to carry a high number of payloads indicates that stable vertical thrust must be prioritized, so only traditional drone configurations were considered. Any lift-generating surfaces were ruled out as over-complex and not beneficial to a mission where a relatively short distance must be covered, and payload deployment must be maximized.

4.4 Payload Mechanism Design Rational

The space of payload dropper mechanism designs was thoroughly explored in the conceptual design phase and compared against customer and derived requirements. To optimize for individually actuated payload release, a modular individual mechanism was chosen over a mechanism that multiplexes electrically or mechanically; this ensures redundancy, simplicity, and minimal single points of failure. Electrically actuated dropper mechanisms were chosen over single-use mechanisms such as nichrome wires for re-usability and testing. High-torque micro servos were determined to optimize weight, supply chain constraints, reliability, and actuation strength. Several variations were considered: linkage-pin mechanisms, pivoting spring mechanisms, and tabbed mechanisms. Many mechanisms require precise alignment, cannot be manually reset, have multiple complicated parts, or could accidentally release payloads. A rotating tab-slot mechanism, described in detail in the Technical Innovations section, was chosen as it excels in the aforementioned categories.

5 Technical Innovations

5.1 Unique Design Considerations and Technologies

5.1.1 Iterative Frame Design

Starting with static loading requirements from propulsion sources and moment arms, we used the SolidWorks Topology Optimization function to find ideal candidate sections for frame weight relief. Based on this visual data, we cycled through an iterative design process following this framework: sketch, FEA, identify areas of weakness and excess strength, and repeat. Final FOS(Factor of Safety): 7.8; Final total deflection: 0.78 mm; Final frame weight: 322 g.

5.1.2 Payload Dropping Mechanism

The individual payload dropping mechanism (Fig. 4) has been optimized to balance weight, manufacturability, durability, and reliability. The mechanism uses a lightweight high-torque MG90S metal-gear servo to rotate the indented servo attachment inside of a TPU-95A slotted housing. The semi-flexible slotted TPU housing protects the rotating shaft assembly from excessive axial radial loads and has enabled the mechanism to survive severe crashes. The TPU housing also mitigates tolerance stackup while ensuring minimal play and vibrations by flexing around the payload tab. The mechanism is failsafe in that precise alignment is not required to keep the payload tab locked in the slot, and the unpowered breakaway torque exceeds any expected inertial payload torque by a factor of 15. Optimizing the infill geometry and perimeter count of the 3D-printed parts allows for a net mechanism weight of only 37 grams. The use of well-tuned 3D printing also ensures scalability, repeatability, and manufacturability.

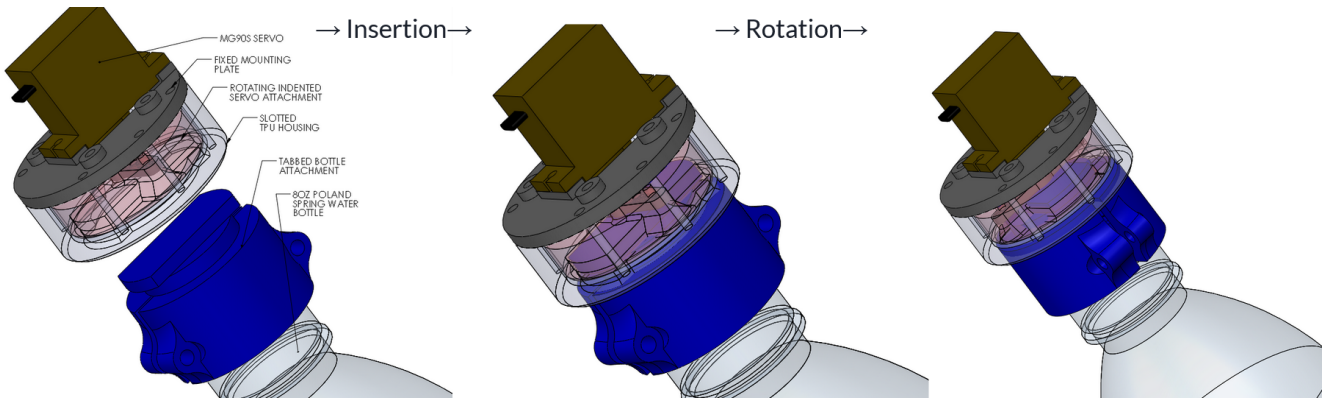

Figure 4: Universal Dropper Attachment System

5.1.3 Companion Computer

A custom companion computer and power system solution was implemented to actuate the 18 dropping servos in an optimized order to minimize CG shifts and maximize delivery accuracy. Leveraging an ESP32 S3 and FreeRTOS, we developed a firmware stack with three main goals: MavLINK communication with the flight controller, Servo

controller, and WiFi connection with the ground station. A semaphore-based approach allows for data to be seamlessly passed through different memory regions without running into race conditions. This was achieved through careful low-level C-based optimizations, mainly focused on increasing the reliability of the UART MavLINK connection. Once communication is established with the Pixhawk the ESP32 is able to arm the servos and can drop the preordered payloads based on pilots input. By preordering the payload drops, we are able to maintain a tighter CG and enhance flight stability. Each of the servos is controlled by 3 LEDC drivers, which calculate the duty cycle and provide PWM to the appropriate servo. The servos remain powered during flight for further redundancy protecting against accidental release. Furthermore, while on the ground and disarmed the payloads can all be immediately locked and unlocked via WiFi or MavLINK commands for easier reloading and deployment. Combining these three tasks into a single firmware stack allows for streamlined testing and a high degree of adaptability.

5.2 Mission Model for System Performance Prediction

A comprehensive mission model was developed to evaluate and compare propulsion system components while predicting mission performance metrics such as endurance, hover capability, and payload capacity. The model integrates aerodynamic, propulsion, environmental, and energy system dynamics to construct an accurate representation of the aircraft's operation across various mission phases. This model serves a dual purpose:

- **Propulsion System Comparison**: Evaluates the efficiency of different motor-propeller-battery configurations by predicting power draw and energy consumption.
- **Mission Performance Prediction**: Estimates achievable mission objectives by computing flight endurance, energy efficiency, and payload constraints.

The optimization process follows a structured workflow to enhance VTOL mission performance. Data pre-processing and interpolation involve extracting motor-propeller performance data from CSV files, including metadata such as motor model, propeller diameter, and mass. Throttle-thrust-current relationships are interpolated within a 40-100% throttle range for smooth function evaluation. Total mass is configured to account for total vehicle mass by summing frame, electronics, payload, battery, and propulsion system weights, with additional weight penalties for the structural requirements of larger propeller diameters. The mission simulation utilizes a numerical differential equation solver to model takeoff, cruise, and landing phases based on Newtonian physics, iterating laps until battery depletion or the time limit is reached. Optimization aims to maximize completed mission laps by refining throttle settings for takeoff and cruise using pattern search, a discontinuous local optimizer with a multistart approach for improved convergence. Linear constraints ensure practical propulsion settings, with a mesh tolerance of 10e6 and a maximum of 500 iterations. Visualization includes hover time vs. payload capacity and battery/time remaining vs. mission laps, along with a stacked bar chart comparing battery depletion and flight time across configurations. This framework systematically evaluates propulsion trade-offs, supporting VTOL design decisions based on energy efficiency, endurance, and operational constraints.

5.2.1 Governing Equations

The mission model is built upon physics-based governing equations that characterize aircraft motion, energy usage, and aerodynamic forces. The system dynamics are defined as follows:

Force Equilibrium in Hover and Cruise

$$W = mg, \quad T_{\text{total}} = nT, T_{\text{req}} = \frac{1}{2}\rho C_d A v^2 + W \sin\theta \tag{1}$$

where W is total weight, T_{total} is total thrust from n motors, and T_{req} represents the thrust required for sustained flight in forward motion. The model interpolates empirical thrust-current curves from motor testing data to determine the required electrical power at different throttle settings.

Energy Consumption and Endurance Estimation The total power draw is obtained from the propulsion system characteristics:

$$P_{\text{total}} = \sum_{i=1}^{n} P_i = \sum_{i=1}^{n} \left(I_i V_{\text{bat}}\right), \quad \text{where } I_i = f(T_i) \tag{2}$$

where P_{total} is the aggregate power consumption, and I_i is the interpolated current draw for a given thrust setting. The corresponding flight endurance is computed as:

$$t_{\text{endurance}} = \frac{C_{\text{bat}}}{I_{\text{avg}}} \tag{3}$$

where C_{bat} is battery capacity (Ah) and I_{avg} is the time-averaged current draw during the mission.

Optimization for Energy-Efficient Flight The optimal throttle setting τ^* is determined via constrained nonlinear optimization, minimizing total energy consumption while ensuring sufficient thrust:

$$\tau^* = \arg\min_{\tau} \int_0^T P_{\text{total}}(\tau)dt, \quad \text{s.t. } T_{\text{req}}(\tau) \geq W \tag{4}$$

MATLAB's `patternsearch` and `fmincon` algorithms are used to numerically compute τ^* across varying mission profiles.

5.2.2 Sources of Model Inputs

The mission model integrates empirical and theoretical data from multiple sources to provide a realistic performance prediction. For aerodynamic approximations, a CEAS Aeronautical Journal article provided [8] estimations of drag coefficients for both the drone body and propellers. Propulsion data supplied by motor manufacturers provided the current-thrust curves and ESC efficiency estimations. Manufacturer discharge curves were used for battery performance and endurance calculations. In addition, location-based environmental factors such as ambient temperature, altitude, and wind data were taken from Weather Underground [9], providing estimates for possible competition conditions.

5.2.3 Assumptions and Uncertainties

The predictive model for the drone system incorporates several simplifications that introduce potential sources of error. In the propulsion system modeling, polynomial interpolation of motor thrust and efficiency curves is used, neglecting transient effects such as dynamic changes during acceleration and deceleration. Additionally, ESC efficiency is assumed to be constant, which may not reflect real-world variations due to factors like temperature and load. The battery is assumed to be ideal. For aerodynamic and environmental factors, the model assumes a fixed drag coefficient (C_d), disregarding potential variations. Wind disturbances, gusts, and turbulence are not modeled, but contained into our safety factor considerations. Introduced error will be addressed empirically and experimentally.

6 Design Definition

6.1 Propulsion System

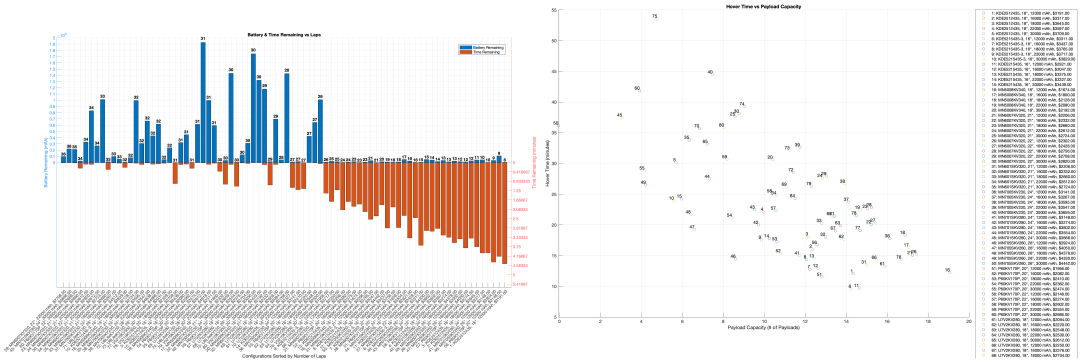

(a) Mission 1 performance

(b) Mission 2 performance

Figure 5: Propulsion modeling results

Figure 5 presents results that informed the selection of propulsion components based on data-driven analysis. The chosen configuration includes the T-Motor Antigravity MN6007II motor, P22 × 6.6" propeller, and a 6S 22,000 mAh battery. This combination is expected to achieve optimal performance, with a projected maximum of 36 laps in Mission 1, a payload capacity of 13 units, and a hover time of 28 minutes, well suited to performance requirements.

6.2 Electronic Systems

The electronics system is defined by its power distribution and consumption, necessitating a modular architecture due to the use of separate batteries. The flight system comprises a 6S 22.2V flight battery, an 8-in-1 ESC, and six BLDC motors. A dedicated electronics battery supplies power to all subsystems excluding the FAA lights and FAA module. Both power systems prioritize safety, incorporating shunt plugs and continuous monitoring mechanisms to ensure operational reliability.

The flight system integrates a custom INA260 power distribution board (PDB), which transmits real-time current and voltage telemetry. The electronics battery supplies power to the flight controller and servo array through buck converters. Given that the servos and flight controller constitute the primary current draw, the buck converter must sustain a continuous output of at least 8A, with a burst tolerance of 10A. To meet these requirements, a custom power regulation solution was developed, employing two buck converters in series. The first buck converter powers servos and subsystems, while the second ensures proper power delivery to the Pixhawk via the INA260 board.

The flight controller utilized in this system is the Pixhawk 6X, which according to its documentation, requires a continuous 3A supply at 5V. This enables the Pixhawk to support critical peripherals, including the camera system, telemetry module, companion computer, and GPS/RTK module. The camera system comprises an FPV camera mounted on a servo, to have the pilot have forward flight views and drop position views. The companion computer serves as an auxiliary telemetry node, transmitting external flight data to the ground station and communicating with the flight controller over UART to determine the appropriate payload deployment sequence.

The telemetry system operates on a Crossfire-based radio protocol, ensuring a stable and reliable communication link for command and control during flight. GPS and RTK positioning provide high-precision navigation, which is critical for accurate payload deployment.

6.3 Lift and Drag Analysis

Glauert's hypothesis provides relationships to find the hexacopter thrust and lift in relation to downwash, induced velocity, and propeller geometry for various stages of flight. [10]

$$T = 2\rho A \bar{V} w \ , \quad \bar{V} = \sqrt{(w - V\sin\alpha)^2 + (V\cos\alpha)^2} \ , \quad w = \frac{2L}{\pi\rho V b^2} \ , \quad L = 2w\rho\left(\pi\frac{b^2}{4}\right)V$$

To analyze these forces in cruise, the lift is equated with the weight of the drone, while a drag estimate can be found by a force summation in the flight direction.

$$L = T\cos\alpha = W \ , \quad T\sin\alpha = D$$

Using an estimate of 20 degrees for the hexacopter's angle of attack in cruise and weight without payloads attached, the team calculated a cruise lift estimate of 16 lb and a cruise drag estimate of 6.2 lb.

6.4 Weight Analysis

A robust weight budget breakdown is necessary to guide design, manufacturing, and material selection such that the aircraft is within the 25 lb fully loaded weight allowance:

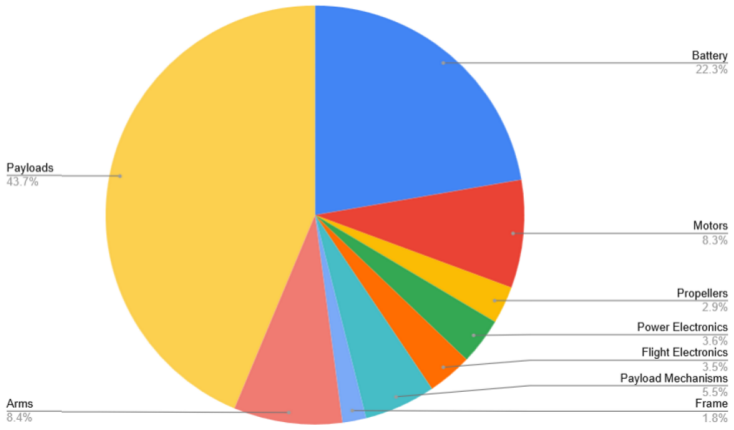

Figure 6: Weight breakdown by percentage

The final hexacopter design mass distribution is approximately axisymmetric, with any asymmetry due to electronic component positioning essentially negligible.

6.5 Structural Analysis

6.5.1 Arm Selection

Tube #	OD (in):	ID (in):	Cost per inch	g/in	Wall Thickness (in):	Arm length (in)	Moment of Inertia (in^4):	Max Moment (in-lbs):	Max Stress (psi):	Max deflection (in)	Factor of Safety:	Total Tube mass (g):	Total tube cost:
1	0.986	0.902	$1.81	3.373	0.042	18.7	0.013902215	216.2994012	7670.404075	9.82E-02	18	378.4347769	$202.82
2	0.981	0.875	$1.50	3.739	0.053	18.7	0.016687603	216.2994012	6357.705012	8.18E-02	22	419.5233811	$168.30
3	1.1	0.99	$3.00	3.780	0.055	18.7	0.024715694	216.2994012	4813.325054	5.52E-02	29	424.1026429	$336.60
4	1.106	1	$1.72	4.046	0.053	18.7	0.024362379	216.2994012	4909.765518	5.60E-02	29	453.9111649	$192.56
5	1.09	1	$1.48	3.688	0.045	18.7	0.020203465	216.2994012	5834.799795	6.75E-02	24	413.8426875	$165.96
6	0.965	0.875	$1.36	3.239	0.045	18.7	0.013793475	216.2994012	7566.219755	9.89E-02	19	363.3748938	$153.11
7	1.07	1	$1.74	2.715	0.035	18.7	0.015256163	216.2994012	7585.142877	8.94E-02	19	304.5832625	$194.79
8	1.09	1	$2.39	3.680	0.045	18.7	0.020203465	216.2994012	5834.799795	6.75E-02	24	412.872797	$267.68
9	1.185	1.101	$1.69	3.780	0.042	18.7	0.024662317	216.2994012	5196.486518	5.53E-02	27	424.1082083	$190.12
10	1.29	1.23	$1.54	2.979	0.03	18.7	0.023579734	216.2994012	5916.653376	5.79E-02	24	334.2220299	$172.49
11	1.374	1.22	$7.34	6.384	0.077	18.7	0.06620618	216.2994012	2244.468534	2.06E-02	63	716.3196751	$823.40
12	1.58	1.5	$2.29	3.868	0.04	18.7	0.057408333	216.2994012	2976.510856	2.38E-02	47	434.03125	$257.13
13	1.83	1.75	$2.40	4.498	0.04	18.7	0.090135482	216.2994012	2195.738546	1.51E-02	64	504.6875	$268.81

Figure 7: Structural calculations for motor arms

6.6 Finite Element Analysis

Our simulations aimed to assess the structural integrity of a system under realistic loading conditions, ensuring that critical components could withstand applied forces while remaining within design constraints.

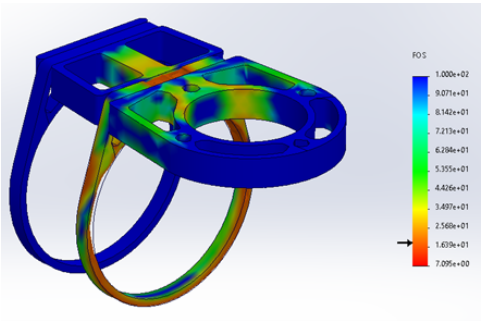

Figure 8: Motor mount FOS

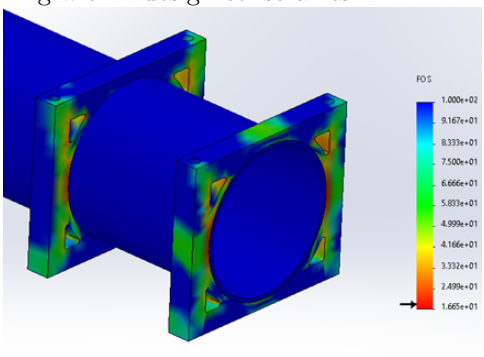

Figure 9: Arm mount FOS

The model included only structurally relevant components, excluding elements that did not significantly impact load distribution. We focused on the motor mounts, arms, frame, and appropriate connectors. Carbon fiber and 7075-T6 Aluminum were selected for the components. Carbon fiber components were assumed to behave isotropically to simplify the study and reduce computation time, while the properties of aluminum were directly imported into the study.

Bolt connectors were used to replicate our fasteners, with preload assumptions incorporated to simulate realistic joint behavior and stress concentrations around the joint. Bonded interactions were used for permanently joined

components, and contact interactions were used to allow for some motion under load for critical components. This ensured accurate stress distribution and realistic load paths within and across components.

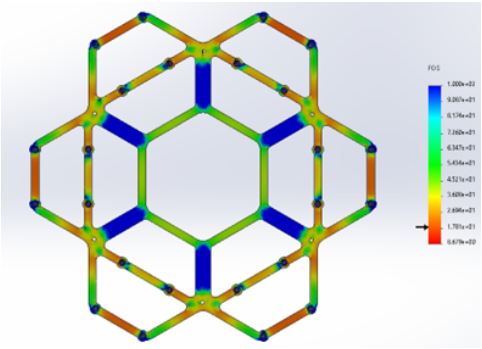

Figure 10: Top frame FOS

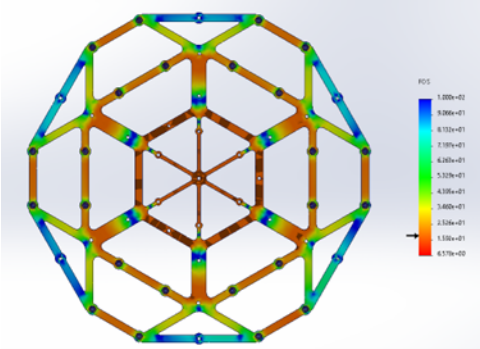

Figure 11: Bottom frame FOS

Three primary load conditions were applied to the structure: the thrust force applied at the mounting points; gravitational acceleration of 2.5 g reflecting high-acceleration takeoff; and additional loads from the weight of motors, electronics, and payloads, spread appropriately across mounting points, reflecting a realistic mass distribution.

A fine mesh was used to maximize resolution, with a blended curvature-based mesh to increase resolution around fillets and curves. Inertial relief was employed during the simulation to simulate the drone in flight, providing realistic data compared an anchored frame simulation.

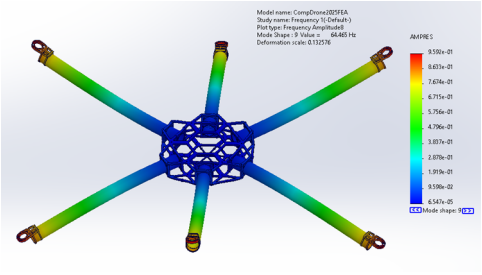

Figure 12: Full drone resonance study

Mode No.	Frequency(Hertz)	Period(Seconds)
7	61.745	0.016196
8	61.749	0.016195
9	64.465	0.015512
10	78.703	0.012706
11	81.033	0.012341
12	81.277	0.012304
13	87.509	0.011427
14	87.512	0.011427
15	243.67	0.0041039

The frequency analysis was also conducted to determine the natural frequencies and structural deflection. This is vital for structural design and control system programming to mitigate resonance behavior. The mass load conditions from the static study were maintained to ensure consistency in mass distribution. Rigid connections were used instead of distributed connections to provide computational efficiency while maintaining the necessary fidelity for accurate frequency predictions.

6.7 Final Dimensional Parameters

Component	Frame Diameter	Arm Length	Arm Diameter	Frame Plates Thickness	Total Arm span	Propeller Diameter
Dimension (in)	11.5	18.7	1.5	0.19	47	22

Figure 13: Weight breakdown by percentage

6.8 Stability Analysis

The hexacopter dynamics can be modeled using a six-degree-of-freedom state variable equation, where the inputs are drone thrust, rolling moment, pitching moment, and yawing moment.

$$
\begin{bmatrix} \dot{u} \\ \dot{v} \\ \dot{w} \\ \dot{p} \\ \dot{q} \\ \dot{r} \\ \dot{\phi} \\ \dot{\theta} \\ \dot{\psi} \\ \dot{x} \\ \dot{y} \\ \dot{z} \end{bmatrix} = \begin{bmatrix} 0 & 0 & 0 & 0 & -w & v & g\sin\theta & 0\,0\,0\,0\,0 \\ 0 & 0 & 0 & w & 0 & -u & -g\cos\theta\sin\phi & 0\,0\,0\,0\,0 \\ 0 & 0 & 0 & -v & u & 0 & -g\cos\theta\cos\phi & 0\,0\,0\,0\,0 \\ 0 & 0 & 0 & 0 & q & -r & 0 & 0\,0\,0\,0\,0 \\ 0 & 0 & 0 & -q & 0 & p & 0 & 0\,0\,0\,0\,0 \\ 0 & 0 & 0 & r & -p & 0 & 0 & 0\,0\,0\,0\,0 \\ 0 & 0 & 0 & 1 & \sin\phi\tan\theta & \cos\phi\tan\theta & 0 & 0\,0\,0\,0\,0 \\ 0 & 0 & 0 & 0 & \cos\phi & -\sin\phi & 0 & 0\,0\,0\,0\,0 \\ 0 & 0 & 0 & 0 & \frac{\sin\phi}{\cos\theta} & \frac{\cos\phi}{\cos\theta} & 0 & 0\,0\,0\,0\,0 \\ \cos\theta\cos\psi & -\cos\theta\sin\psi & \sin\theta & 0 & 0 & 0 & 0 & 0\,0\,0\,0\,0 \\ \sin\psi & \cos\psi & 0 & 0 & 0 & 0 & 0 & 0\,0\,0\,0\,0 \\ -\cos\psi\sin\theta & \sin\psi\sin\theta & \cos\theta & 0 & 0 & 0 & 0 & 0\,0\,0\,0\,0 \end{bmatrix} \begin{bmatrix} u \\ v \\ w \\ p \\ q \\ r \\ \phi \\ \theta \\ \psi \\ x \\ y \\ z \end{bmatrix} + \begin{bmatrix} 0 & 0 & 0 & 0 \\ 0 & 0 & 0 & 0 \\ \frac{1}{m} & 0 & 0 & 0 \\ 0 & \frac{1}{I_x} & 0 & 0 \\ 0 & 0 & \frac{1}{I_y} & 0 \\ 0 & 0 & 0 & \frac{1}{I_z} \\ 0 & 0 & 0 & 0 \\ 0 & 0 & 0 & 0 \\ 0 & 0 & 0 & 0 \\ 0 & 0 & 0 & 0 \\ 0 & 0 & 0 & 0 \\ 0 & 0 & 0 & 0 \end{bmatrix} \begin{bmatrix} T \\ M_x \\ M_y \\ M_z \end{bmatrix}
$$

Since a hexacopter aircraft configuration is not statically stable, the drone uses an active PID control system for dynamic stability. As shown in the system block diagram, the feedback loop incorporates the IMU data with RTK module position comparison to eliminate drift. It was determined that the installation of an RTK module was necessary to eliminate position drift for targeting in the competition.

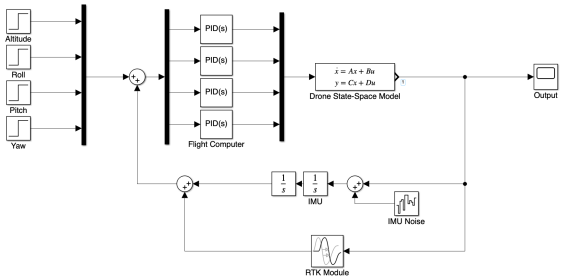

Figure 14: Control system diagram.

7 Drawing Package

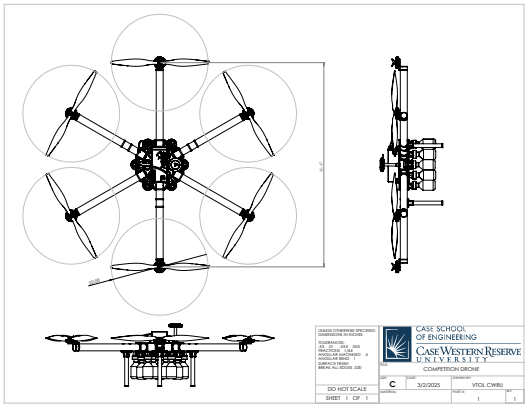

(a) Orthogonal views

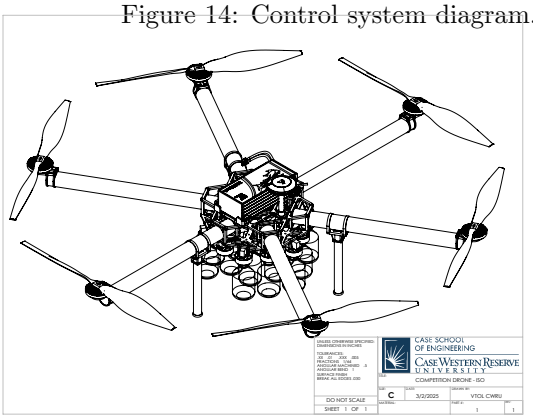

(b) Isometric view

Figure 15: Aircraft Drawings

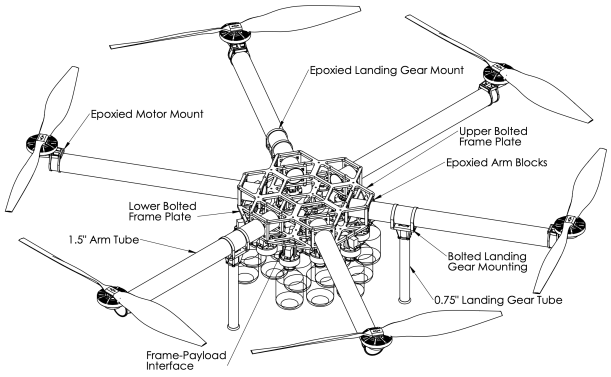

(a) Structural arrangement diagram

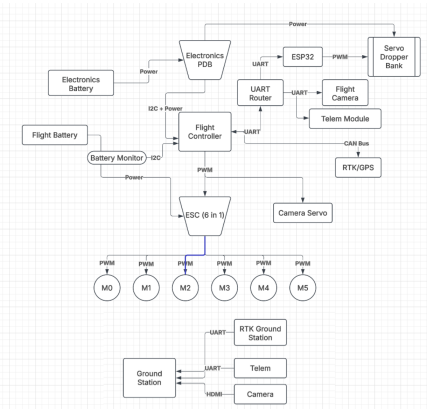

(b) System Interconnect Diagram

Figure 16

8 Fabrication Methods

8.1 Manufacturing Processes

8.1.1 Frame

For the central frame, we evaluated various thicknesses of 7075 aluminum, 6061 aluminum, and carbon fiber plates for their strength-to-weight ratio, stiffness, and dynamic stress tolerance. After extensive testing, as detailed in section X, we selected 7075 aluminum. We chose waterjet cutting for all aluminum components due to its simplicity, capability to create complex 2D geometry in high-strength materials, and ease of DXF file creation. However, due to waterjet machine issues and build timeline constraints, we used a CNC mill for several parts. While CNC milling provided better tolerances, it required more complex toolpath creation.

8.1.2 Structural Connections

For all of our structural connections, we considered 3D printed PLA, PETG, and PLA+, as well as aluminum. These materials were considered for manufacturability, low cost, and strength properties. Ultimately all structural connections were made from 7075-T6 waterjet aluminum of thicknesses ranging from 1/8 to 1/2 inch. This choice provides maximum FOS for load-bearing components while maintaining manufacturability and economic feasibility. For example, the motor mount plates are first waterjet, and then channels are precisely manually milled in order to fit other epoxied aluminum connections.

8.1.3 Arms

For the arms, we considered circular and square tubing of 7075-T6 aluminum, carbon-kevlar composite, and carbon fiber composite. These materials were considered for their high torsional strength. Ultimately, carbon fiber composite tubes were chosen based on their higher stiffness-to-volume ratio, minimizing deflection. The tubing was cut to length using a custom jig to avoid tube crushing and a diamond composite blade on a horizontal bandsaw.

8.1.4 Non-structural Connections

For non-structural connections and mounting we used mainly standard PLA 3d prints. 6061 aluminum was considered for this application but was rejected due to complex manufacturing with little benefit. Most often, mounting requires complex geometry, which cannot be easily completed on the water jet/manual milling. PLA 3d prints were chosen for manufacturability and low cost. For shock-absorbing components like landing gear connection points, PETG 3d prints were used for its unique mechanical properties.

9 Test Plan

9.1 Ground Testing

Objective: Determine if all electrical, structural, and connectivity systems are fully secured, robust, and correctly assembled.
Test Setup: The initial ground and components test will be conducted with props removed for safety. The drone will be connected to Mission Planner over a USB connection with the electronics battery connected to ensure power to all flight control and communication systems. The drone will be manipulated physically while observing the Mission Planner Data tab artificial horizon. After confirming all directions (Roll, Pitch, and Yaw) are correct, communication systems are tested. The Crossfire receiver and transmitter are turned on, and stick inputs and switches are checked in the Radio Calibration tab of Mission Planner. Vital telemetry data such as battery voltage, current draw, and GPS ground speed are verified. Control inputs are reversed in Mission Planner if necessary.

After confirming and correcting motor direction prior to the general test, motors are brought up to 30% of their total PWM values for one minute. Manufacturer prop and motor data are compared to ensure safe RPM and ESC temp limits. Once passed, the drone is disconnected from the configurator and battery, propellers are installed, and the aircraft is rebooted to simulate pre-flight conditions and normal startup.

9.2 Initial Hop and Hover Endurance Test (Takeoff/Landing)

Test Objectives: Determine takeoff and landing characteristics and real-world battery performance to compare with predicted values.
Test Setup: The hover test will be performed at Case Western Reserve University's Van Horn Field. The proper LAANC authorization and remote ID modules are installed and activated. A Part 107-certified team member will fly or be present as the remote pilot in command. The test starts with the same ground test checklist but with propellers installed. Before arming, the drone is switched to a stabilized flight mode to limit bank angle and drift. The drone is then armed, and propellers are spun at 5-10% throttle. The pilot in command ensures that all propellers are rotating at the same speed. Quick pitch and roll inputs are performed to confirm stick directions before lifting off.

The drone is flown in stabilized mode up to 5-10 meters off the ground. The pilot then performs initial maneuvers and lands. After the initial hop, the pilot takes off again and holds position 10 meters above the ground until the predetermined minimum battery voltage is reached. The drone is then landed, disarmed, and the shunt plug removed. Collected data includes total hover time, milliampere-hour draw, ESC amp draw, and starting and final battery voltage, all extracted from flight controller logs.

9.3 Tuning Flights

Objective: Tune PID controllers and response to improve flight dynamics and stability to external disturbances.
Test Setup: Within ArduPilot, Autotune flight mode is assigned to a switch on the radio. A fully charged battery is used, and additional payloads and camera equipment are removed for maximum flight time. The pilot in command completes the flight checklist and takes off in stabilized mode. The drone is then switched into Autotune flight mode. During Autotuning, the UAV performs a series of quick automated maneuvers in the order of roll, pitch, and then yaw. Once completed, the flight controller updates the PID loops based on data collected from the Autotune mode. The changes are verified in logging before performing another flight.

A confirmation flight is conducted to ensure improvements in response and stability. This flight includes full deflection pitch and roll maneuvers, as well as high-throttle climbs.

9.4 Mission Systems Integration Test

Objective: Evaluate the performance of mission-specific hardware and software under mission conditions.
Test Setup: Mission-specific hardware and payloads, including the dropper assembly and associated electronics, are installed. A mock mission (Mission 3) is set up on a test field with three different-sized targets. The pilot in command completes a lap of Mission 3 using FPV goggles for flight. Drop sections use the downward-facing view of the servo-mounted camera. After landing, team members record any drop system issues, such as drop delays, premature drops, or stuck droppers. Drop accuracy and scoring are also recorded before another attempt.

10 Test Results

Outcome: The competition drone manufacturing and assembly is still in progress; after completion, the aforementioned tests will be used to evaluate post-production performance and changes. Our secondary testing quadcopter was essential in creating the official process to tune and set parameters. This will greatly minimize the experimental tuning and time spent on the final drone. The following sections elaborate on the quantitative metrics and qualitative results obtained from the testing process of the test drone.

10.1 Tuning:

We performed a total of three tuning flights of 5 to 8 minutes each; each flight adjusted the parameters of a different principal axis. Roll was the first adjusted axis, followed by pitch, and then yaw. Each tuning procedure sent precise inputs to the ESCs and motors—the drone would make adjustments and then store the updated PID values in the onboard memory. Each of our tuning flights successfully adjusted the necessary parameters and made the flight substantially more stable. Pre-auto tuning flights were shaky, unstable, and had very low resistance to external wind disturbances, which caused several unexpected crashes. After the autotuning procedure, the test drone was steady and more resistant to wind. Autotune flight mode made the vehicle altitude-hold when activated. We expect the procedure of autotuning on the competetion drone to be similar to our test drone. However there may be more intricacies associated with a heavier drone with 6 motors.

10.2 Structural and Crash Testing:

After each flight, a visible inspection was performed to evaluate the structural condition of all major components. Additionally, several major crashes were inadvertently induced throughout the test drone's flights and autotuning process. Before we conducted the tuning process, most crashes were caused by. After we conducted the tuning process, the main reason for crashing was because of instable flight due to oscillations and instability in wind gusts. After the tuning, instability-related crashes were eliminated, with the few remaining incidents attributed to pilot error. The landing gear was highly susceptible to inadvertent lateral movements during landing and would break easily. Changes were made to the 3D print layer orientation, and the issue was resolved. This informed our decision-making on 3D printed part design for the competition hexacopter.

Figure 17: Test drone used for flight evaluation and system integration.

10.3 Payload drop testing:

Four dropper mechanisms identical to the competition drone mechanism were installed on the test drone and used to practice drops within mock mission target areas. A downward-facing FPV camera was utilized to approach and line up with the targets. Drop accuracy and dropper mechanism robustness were evaluated.

10.4 Final Flight Observations:

The test drone's post-tuning flights demonstrate a stable hover around 45-55 percent throttle. The test drone holds altitude well, and there are no observable oscillations. Drift occurs in moderately strong wind gusts, but the movements are manageable. Full stick deflection inputs were tested in stabilized mode (30-degree pitch and yaw) with no oscillations of difficulty returning to hover afterward. Based on these results from the test drone, the competition drone should have improved resistance to wind disturbances because of its increased weight, additional propellers, and associated propeller disc area.

Figure 18: FPV view of the payload dropping from the drone.

11 Bibliography

[1] 2025, Satellites Monitor California Wildfires, NOAA, from: https://www.nesdis.noaa.gov/news/noaa-satellites-monitor-california-wildfires

[2] Allison Et al, 2016, "Airborne Optical and Thermal Remote Sensing for Wildfire Detection and Monitoring." National Library of Medicine,27548174, from: https://pmc.ncbi.nlm.nih.gov/articles/PMC5017475/

[3] 2022,"Community Wildfire Defense Grant Program." USDA, from: https://www.fs.usda.gov/managing-land/fire/grants/

[4] Daley, 2017, "Study Shows 84% of Wildfires Caused by Humans." Smithsonian, from: https://www.smithsonianmag.com

[5] "Snake Safety." USDA, from: https://www.fs.usda.gov

[6] 2023, "USDA Forest Service announces nearly $19M to fight invasive species threatening nation's forests." USDA, from: https://www.fs.usda.gov

[7] 2024, "Economic risks: Forest Service estimates costs of fighting wildfires in a hotter future." USDA, from: https://www.fs.usda.gov

[8] Hammer Et al., 2024, "Free fall drag estimation of small-scale multirotor unmanned aircraft systems using computational fluid dynamics and wind tunnel experiments.", *CEAS AERONAUTICAL JOURNAL* , Vol.15, pp.269–282.]

[9] "Churchville MD, Weather History." WeatherUnderground, from: https://www.wunderground.com

[10] McCormick, B. W., 1995, Aerodynamics, Aeronautics, and Flight Mechanics, 2nd ed., Wiley, New York.